Surface pattern formation and scaling described by conserved lattice gases

Géza Ódor,[1] Bartosz Liedke,[2] and Karl-Heinz Heinig[2]
[1]*Research Institute for Technical Physics and Materials Science, P.O. Box 49, H-1525 Budapest, Hungary*
[2]*Institute of Ion Beam Physics and Materials Research, Forschungszentrum Dresden–Rossendorf, P.O. Box 51 01 19, 01314 Dresden, Germany*

(Received 15 December 2009; revised manuscript received 26 February 2010; published 12 May 2010)

We extend our 2+1-dimensional discrete growth model [Ódor *et al.*, Phys. Rev. E **79**, 021125 (2009)] with conserved, local exchange dynamics of octahedra, describing surface diffusion. A roughening process was realized by uphill diffusion and curvature dependence. By mapping the slopes onto particles, two-dimensional nonequilibrium binary lattice model emerges, in which the (smoothing or roughening) surface diffusion can be described by attracting or repelling motion of oriented dimers. The binary representation allows simulations on very large size and time scales. We provide numerical evidence for Mullins-Herring or molecular-beam epitaxy class scaling of the surface width. The competition of inverse Mullins-Herring diffusion with a smoothing deposition, which corresponds to a Kardar-Parisi-Zhang (KPZ) process, generates different patterns: dots or ripples. We analyze numerically the scaling and wavelength growth behavior in these models. In particular, we confirm by large size simulations that the KPZ type of scaling is stable against the addition of this surface diffusion, hence this is the asymptotic behavior of the Kuramoto-Sivashinsky equation as conjectured by field theory in two dimensions, but has been debated numerically. If very strong, normal surface diffusion is added to a KPZ process, we observe smooth surfaces with logarithmic growth, which can describe the mean-field behavior of the strong-coupling KPZ class. We show that ripple coarsening occurs if parallel surface currents are present, otherwise logarithmic behavior emerges.

DOI: 10.1103/PhysRevE.81.051114 PACS number(s): 05.70.Ln, 05.70.Np, 82.20.Wt

I. INTRODUCTION

In nanotechnologies, large areas of nanopatterns are needed, which can be fabricated today only by expensive techniques, e.g., electron-beam lithography or direct writing with electron and ion beams. Besides the conventional "top-down" technologies, which use masks, photoresists, etc. to create structures on the surfaces, nowadays "bottom-up" approaches are getting close to achieve the same results more efficiently. In that case, the self-assembly of patterns of large areas is facilitated in a cost effective way [1]. This has led reopening of the research for fundamental theoretical understanding of the ion-beam-induced surface patterning and scaling [2], which was flourishing at the end of the previous century [3,4]. Although the basic universality classes and important models have been explored, many notoriously difficult fundamental questions have been unanswered. Perturbative renormalization-group methods and analytical tools have limited applicability and precise numerical simulations, approaching asymptotic scaling regimes, were feasible in one dimension mainly.

One of the most fundamental problems of kinetic roughening can be characterized by the Kardar-Parisi-Zhang (KPZ) equation [5]. The KPZ has been found to describe other important physical phenomena such as randomly stirred fluid [6], dissipative transport [7,8], directed polymers [9], and the magnetic-flux lines in superconductors [10]. Therefore, we started our studies by setting up the simplest possible microscopic model exhibiting this behavior [11,12].

The KPZ is a nonlinear stochastic differential equation, describing the dynamics of growth processes in the thermodynamic limit specified by the height function $h(\mathbf{x},t)$,

$$\partial_t h(\mathbf{x},t) = v + \sigma\nabla^2 h(\mathbf{x},t) + \lambda_2[\nabla h(\mathbf{x},t)]^2 + \eta(\mathbf{x},t). \quad (1)$$

Here, v and λ_2 are the amplitudes of the mean and local growth velocities, respectively, σ is a smoothing surface-tension coefficient, and η roughens the surface by a zero-average, Gaussian noise field exhibiting the variance

$$\langle \eta(\mathbf{x},t)\,\eta(\mathbf{x}',t')\rangle = 2D\delta^d(\mathbf{x}-\mathbf{x}')(t-t'). \quad (2)$$

We denote the spatial dimensions of the surface by d and the noise amplitude by D. The pure KPZ equation is exactly solvable in $1+1d$ [9], but in higher dimensions only approximate solutions are available (see [4]). In $d>1$ spatial dimensions due to the competition between the roughening and smoothing, models characterized by Eq. (1) exhibit a roughening phase transition between a weak-coupling regime ($\lambda_2 < \lambda_2^*$), governed by the $\lambda_2=0$ Edwards-Wilkinson (EW) fixed point [13], and a strong-coupling phase. The strong-coupling fixed point is inaccessible by perturbative renormalization method. Therefore, the KPZ phase space has been the subject of controversies and the value of the upper critical dimension is an active field of studies for a long time.

Mapping of surface growth onto reaction-diffusion system allows effective numerical simulations and better understanding of basic universality classes [14–16]. The principal aim of this paper is to show that some of most fundamental growth processes can be well described by the simplest, restricted solid on solid (RSOS) model with $\Delta h = \pm 1$. This strong condition enables a mapping onto binary lattice gases and facilitates to create fast algorithms. We will discuss models, which follow universal scaling laws and exhibit pattern formation. Although the understanding of coarsening phenomena [17] of surface patterns has been developing rapidly by continuum approaches [18] and the agreement with the

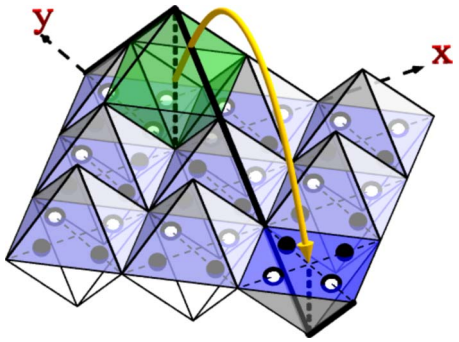

FIG. 1. (Color online) Mapping of the 2+1-dimensional surface diffusion onto a 2d particle model (bullets). Surface attachment (with probability p) and detachment (with probability q) correspond to Kawasaki exchanges of particles or to anisotropic migration of dimers in the bisectrix direction of the x and y axes. The crossing points of dashed lines show the base sublattice to be updated. Thick solid line on the surface shows the y cross section, reminding us to the one-dimensional rooftop model. When the shown desorption or absorption steps are executed simultaneously, they realize a surface diffusion step of size $s=3$ along the y axis. This corresponds to a pair of dimer movement, a repulsion in case of this smoothing reaction.

ion-beam-induced nanopattern experiments is improving [19], the identification of the various coarsening scenarios is still a theoretical challenge [20]. Our approach is based on the KPZ models we presented very recently [11,12], hence for the sake of completeness, we review them now.

In one dimension, a discrete RSOS realization of the KPZ growth is equivalent [21,22] to the asymmetric simple exclusion process (ASEP) of particles [23], while we have shown that this "rooftop model" can be generalized to higher dimensions [11,12]. This mapping is interesting not conceptually only, linking nonequilibrium surface growth with the dynamics of driven lattice gases [24,25], but provides an efficient numerical simulation tool for investigating debated and unresolved problems.

The surface built up from the octahedra can be represented by the edges meeting in the up or down middle vertexes (see Fig. 1). The up edges, in $\chi=x$ or $\chi=y$ directions at the lattice site i,j, are represented by $\sigma_\chi(i,j)=+1$, while the down ones by $\sigma_\chi(i,j)=-1$ slopes. Therefore, we approximate surfaces using RSOS model with $\Delta h=\pm 1$.

In this paper, we show that one can describe various, more complex surface process without the need of having larger Δh height differences. These are built up from the basic octahedron deposition or removal processes [11]. Let us remind the reader that a single-site deposition flips four edges, which means two "+1" $\leftrightarrow$ "−1" (Kawasaki) exchanges: one in the x and one in the y direction. This can be described by the generalized Kawasaki update

$$\begin{pmatrix} -1 & 1 \\ -1 & 1 \end{pmatrix} \underset{q}{\overset{p}{\rightleftharpoons}} \begin{pmatrix} 1 & -1 \\ 1 & -1 \end{pmatrix}, \tag{3}$$

with probability p for attachment and probability q for detachment.

We can also call the +1's as particles and the −1's as holes living on the base square lattice, thus an attachment or detachment update corresponds to a single-step motion of an oriented dimer in the bisectrix direction of the x and y axes. We update the neighborhood of the sublattice points, which are the crossing points of the dashed lines. In [11,12], we derived how this mapping connects the microscopic model to the KPZ equation and investigated the surface scaling numerically. Our best estimates obtained by simulations up to sizes $L=2^{15}$ for the two-dimensional KPZ universality class is in agreement with the operator product expansion result [26]

$$\alpha = 0.395(5), \quad \beta = 0.245(5), \quad z = 1.58(10), \tag{4}$$

within error margin [12].

Besides presenting some more interesting results about the universal scaling behavior of KPZ in this paper, we move further and extend our mapping for describing more complex surface reactions. In particular, we investigate models with surface diffusion processes, which are relevant in material science. We show the emergence of patterns and follow their coarsening dynamics.

A. Simulations

Although the bit-coded simulations are run on the underlying conserved lattice gas of size $L\times L$, starting from $h_{1,1}=1$, we reconstruct the surface heights from the differences

$$h_{i,j} = \sum_{l=1}^{i} \sigma_x(l,1) + \sum_{k=1}^{j} \sigma_y(i,k) \tag{5}$$

at certain sampling times (t), selected with power-law increasing time steps, and calculate its width

$$W(L,t) = \left[\frac{1}{L^2} \sum_{i,j}^{L} h_{i,j}^2(t) - \left(\frac{1}{L^2} \sum_{i,j}^{L} h_{i,j}(t) \right)^2 \right]^{1/2}. \tag{6}$$

In the absence of any characteristic length, the surface is expected to follow Family-Vicsek scaling [27] when we start from a flat initial condition

$$W(L,t) \propto t^{\beta}, \quad \text{for} \quad t_0 \ll t \ll t_s, \tag{7}$$

$$\propto L^{\alpha}, \quad \text{for} \quad t \gg t_s. \tag{8}$$

Here, α is the roughness exponent for $t \gg t_s$ when the correlation length has exceeded the linear system size L and β is the surface growth exponent, which describes the time evolution for earlier (nonmicroscopic $t \gg t_0$) times. The dynamical exponent z can be expressed by the ratio

$$z = \alpha/\beta. \tag{9}$$

However, in case of pattern formation, multiscaling is present in the system and the roughness exponent calculated in different window sizes is not constant and satisfies a different, anomalous scaling law (see [28,29]).

The morphology of pattern formation in experiments is usually followed by the measurement of some characteristic size, e.g., the wavelength in periodic structures, which

evolves nontrivially with time. We can easily define and measure such quantity in our model. By following the up or down slopes in the x direction, we have strings of 1's or -1 of length s_k in the kth slice of the lattice gas in the y direction. We shall characterize patterns by calculating the (y) average of the longest s_k value

$$\lambda = 1/L\sum_{k=1}^{L} \max(s_k). \tag{10}$$

This characteristic length, corresponds to the longest x slope or to the slowest x mode in the Fourier decomposition, will provide information about scaling of the wavelength in our analysis.

By the simulations, we apply periodic boundary conditions in both directions and start from the flat space corresponding to a zig-zag configuration of the slopes (see Fig. 1), therefore, it has a small initial width $W^2(L,0)=1/4$. Before the scaling analysis, we always subtract this constant, being the leading-order correction, from the raw data. Averaging was done usually for 100–200 samples for each parameter value.

In practice, each lattice site can be characterized by the 16 different local slope configurations, but we update it only when the condition (3) is satisfied. Furthermore, due to the surface continuity, not all configurations may occur and we can describe a lattice site by using only two bits. This permits efficient storage management in the memory of the computer and large system sizes. The updates can be performed by logical operations either on multiple samples at once or on multiple (not overlapping) sites at once. Our bit-coded algorithm proved to be ~40 times faster than the conventional FORTRAN 90 code. A crucial point is to use a good, high-resolution random number generator because in case of the $p=1$ KPZ process, the only source of randomness is the site selection, which must be done in a completely uniform way. Otherwise, we realize a KPZ with quenched disorder which belongs to a different universality class (see [16]). We used the latest Mersenne-Twister generator [30] in general, which has very good statistical properties and which is very fast, especially by the SSE2 instructions. But we tested our results using other random number generators as well.

An elementary Monte Carlo step (MCS) starts with a random site selection. This is followed by testing if the place is appropriate for update i.e., "rooftop" for detachments or "valley bottom" for attachment (3). The update is done with the prescribed p and q probabilities and the time is incremented by $1/L^2$, such that one MCS corresponds to a full lattice update. Throughout the paper, we use this unit of time.

B. Generalizations of the octahedron model

An obvious first step is to combine the deposition and the removal processes creating a conserved dynamics. A simultaneous octahedron detachment and deposition in the neighborhood can realize an elementary diffusion step. Surface diffusion is a much-studied basic process [28]. Several atomistic models have been constructed and investigated with the aim of realizing Mullins-Herring (MH) diffusion [31,32] and scaling (for a recent review, see [33]).

The Langevin equation of MH is a linear one, with a ∇^4 lowest-order gradient term

$$\partial_t h(\mathbf{x},t) = \nu_4 \nabla^4 h(\mathbf{x},t) + \eta(\mathbf{x},t), \tag{11}$$

emerging as the result of a curvature-driven surface current $j(\mathbf{x},t) \propto \nabla[\nabla^2 h(\mathbf{x},t)]$, which obeys the conservation law

$$\partial_t h(\mathbf{x},t) + \nabla j(\mathbf{x},t) = \eta(\mathbf{x},t). \tag{12}$$

Here, the noise $\eta(\mathbf{x},t)$ is a nonconserved, Gaussian white one, which can be the result of fluctuations in the ion-beam intensity directed against the surface. This equation is exactly solvable and exhibits a scaling invariance of the roughness characterized by the exponents

$$\alpha = (4-d)/2, \quad \beta = (4-d)/8, \quad z = 4 \tag{13}$$

below the upper critical dimension $d_c=4$.

Microscopic models realizing this behavior are mainly unrestricted solid on solid (SOS) type, which can provide steep slopes and strong curvatures necessary for the $\alpha \geq 1$ roughness exponent in one and two dimensions. However, it turned out that the asymptotic universality class of the various limited mobility growth models is a surprisingly subtle issue. Many of the earlier findings proved to be incorrect due to pathologically slow crossover and extremely long transient effects [34]. Anomalous scaling, by which the local and global behaviors are different, has been found to be relevant in such "superrough" models, where large local slopes are present [29,35–39]. In fact, according to our knowledge, only the "larger curvature (or Kim-Das Sarma) model" [40,41] and the "$n=2$ model" of [42] exhibit MH universality class scaling asymptotically.

The scaling in other "atomistic" models crosses over to behavior dictated by more relevant terms in the sense of renormalization group. This can be the EW class if $\nabla^2(h)$ [43] is present or the molecular-beam epitaxy (MBE) class in case of the fourth-order nonlinearity $\nabla^2[\nabla(h)^2]$ [44–47] [77]. The nonlinear MBE equation

$$\partial_t h = \nu_4 \nabla^4 h + \lambda_{22} \nabla^2 [\nabla(h)^2] + \eta, \tag{14}$$

with nonconserved, Gaussian noise η is just the conserved version of KPZ (CKPZ) and exhibits the following scaling exponents:

$$\alpha = (4-d)/3, \quad \beta = (4-d)/(8+d), \quad z = (8+d)/3. \tag{15}$$

As we can see, all exponents are smaller than those of the linear MH (13) class values and differ from those of the two-dimensional KPZ class (4) significantly.

Here we present RSOS models with $\Delta h = \pm 1$ height restriction within the framework of our previous approach [11], which in the limit of weak external noise exhibit MH or MBE scaling. Due to the simple construction, these can be mapped onto lattice gases of diffusing dimers, allowing an easier way to study the effects of MH and MBE subprocesses of more complex system. Earlier less restrictive RSOS models were used to describe these classes especially in one dimension (for a review, see [33]).

A further step in generalizing our surface models will be the combination of different subprocesses resulting in nonequilibrium system. For example, by adding a competing MH diffusion to the KPZ updates, one can model the noisy Kuramoto-Sivashinsky (KS) equation [48,49]

$$\partial_t h = v + \sigma\nabla^2 h - \nu_4\nabla^4 h + \lambda_2(\nabla h)^2 + \eta. \tag{16}$$

Here, the surface-tension coefficient σ is negative (in contrast with the KPZ), whereas ν_4 is a positive surface diffusion coefficient. However, in our simulations, we realize a gauge-transformed situation: normal KPZ (with positive σ) competing with an inverse MH (iMH) with negative ν_4 [78]. In KS, even the deterministic variant (η=0) exhibits spatiotemporal chaos and is useful to describe pattern formation, such as chemical turbulence and flame-front propagation [48]. There are other physical systems, including ion sputtering, where the noisy version of the KS equation is used [50]. In one dimension, field theory has proved that KS belongs to the 1+1-dimensional KPZ universality class [50]. However, in higher dimensions, perturbative field theory cannot access the strong-coupling fixed point. Numerical studies [51–53] have provided controversial results in 2+1 dimensions, hence it remained a controversial and challenging problem to clarify the asymptotic scaling behavior of KS [54–57].

It was pointed out [58,59] that grooved phases and growth instabilities may emerge as the consequence of broken detailed balance condition

$$P(\{i\})w_{i\to i'} = P(\{i'\})w_{i'\to i}, \tag{17}$$

where $P(\{i'\})$ denotes the probability of the state $\{i\}$ and $w_{i\to i'}$ is the transition rate between states $\{i\}$ and $\{i'\}$. This means that complex structures and patterns can emerge in nonequilibrium system. In one dimension, a model of massive particles exhibiting momentum has been shown to exhibit KS scaling behavior [60]. Later, another one-dimensional RSOS growth model was constructed [61], in which deposition and diffusion of single adatoms were competing. It was suggested that large-scale behavior could be described by the noisy KS equation.

II. REALIZING THE MBE SURFACE DIFFUSION

As we have mentioned in Sec. I, we generate surface diffusion as the simultaneous adsorption-desorption of octahedra. Therefore, in our model, after an appropriate removal site (a rooftop) selection has been done, we search for a valley bottom place in the neighborhood for deposition. The target site is chosen in the $\pm x$ or $\pm y$ direction, with the probabilities p_{+x}, p_{-x} or p_{+y}, p_{-y}, respectively (see Fig. 1). Throughout of our studies, we normalized the attempt probabilities. The maximal jump distance was fixed to be $l_m \leq 4$ lattice units following computer experiments. According to the construction, the nearest-neighbor jump, corresponding to intralayer diffusion, requires $l_m=2$, while larger jump sizes allow intralayer transport. To create MBE or MH behavior, we must allow interlayer transport. Considering jumps with $l_m \geq 3$ does not make difference in the scaling, larger jumps describe faster diffusion on the expense of more CPU time. Having no *a priori* knowledge of the distance dependence of jump sizes and expecting insensitivity of universal scaling on the rates of short-ranged interactions, we used a constant probability for each direction (for more discussion see Sec. II A).

To control this kind of surface diffusion, we impose additional constraints for the accepting a move. We have tried two kinds of rules based on the local neighborhood configurations. The first one is very simple and requires that the height of a particle at the final state is higher than that of its initial site

$$h_{fin} - h_{ini} \geq 0, \tag{18}$$

which makes a surface rougher (inverse or roughening diffusion). The second one is based on the local curvature at the update sites as will be discussed in Sec. II B.

A. Larger height octahedron diffusion model

By this simple condition, we expect to generate rough surfaces of large curvatures, since an octahedron jumping to a higher position has usually smaller number of neighbors in the lateral direction (in this model, we do not allow particles to evaporate from the bottom of a V-shaped valley). In the language of lattice gases, regions of large curvature and maximal slope correspond to large regions of dense particles and holes. An attractive interaction of the dimer moves enhances such segregation. Contrary, we can realize a smoothing or normal diffusion when we accept jumps with the condition $h_{fin}-h_{ini}\leq 0$.

By increasing the local heights, the formation of pyramid-like structures, unstable growth, occurs similarly as in the $n=2$ SOS model [42], but in our case the slopes are limited to 45°. However, by appropriate length rescaling any sharp, continuous surface can be approximated. In the forthcoming, we will investigate both the inverse and the normal diffusion cases and call it the larger height octahedron diffusion (LHOD) model.

Starting from a zig-zag initial condition, corresponding to the flat surface, the hopping with the condition (18), one can make the surface rougher, however, after the slopes of size l_m are developed, the evolution stops because the octahedra are not allowed to pass longer 45° gradient sections (see Fig. 2). To overcome this, we have been trying to allow arbitrarily long jump sizes (nonlocal model), with different, heuristic jump distance-dependent probability functions. We did not find an appropriate one that could produce the expected MH scaling behavior, instead we realized Lévy flightlike models with anomalous diffusion [62] exhibiting nonuniversal scaling. In the light of recent field theoretical interest [63], these can also be the target of further investigations.

However, nonlocal models are rather complex and connection to reality is not always straightforward. Therefore, we followed another strategy by adding a small amount of extra randomness of EW type to our short-range, binary RSOS model. This means the addition of random adsorption or removal events with small probability $p=q \ll 1$ among the LHOD updates. Such events can break up the barriers by splitting up the long monotonous slopes built by the LHOD

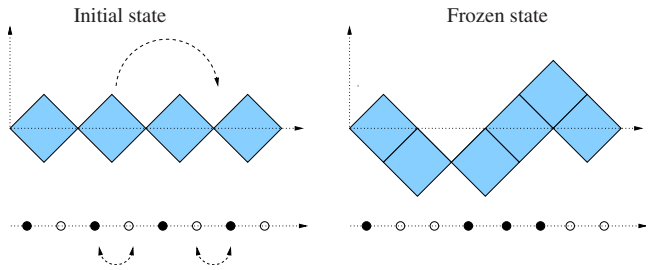

FIG. 2. (Color online) One-dimensional view of a diffusion hop of octahedra by three lattice units to the right. The slopes mapped onto the lattice gas shown below the surface. This roughening surface diffusion move corresponds to two simultaneous, attracting Kawasaki exchanges of the gas (dimers in two dimensions). Starting from the flat (zig-zag) initial state of the pure octahedron model, the (18) process freezes following slopes of maximal length are developed, which cannot be overjumped.

dynamics. If they are done very rarely, i.e., with less than 100 times smaller probability than the diffusion attempts, they can influence the very late asymptotic scaling behavior only, causing an ultimate crossover to the EW class (see, for example, [64]).

In reality, and in the models we are about to study, such randomizing effects are always present, thus we are satisfied, if we can confirm numerically the MBE scaling for intermediate times. It was not our principal aim to provide a model, which exhibits pure MBE type of scaling in the thermodynamic limit. Therefore, we have performed computer experiments on these models as discussed below.

We found that the addition of the small (EW) noise ($p=q \ll 1$) sustains the surface currents and in case of spatially anisotropic diffusion ($p_{+x}=1$, $p_{-x}=p_y=p_{-y}=0$), the scaling becomes Mullins-Herring type [see Fig. 3(a)], characterized by the exponents $\alpha=1$, $\beta=1/4$, and $z=4$ in two dimensions. The collapse of curves is very good in the vertical direction,

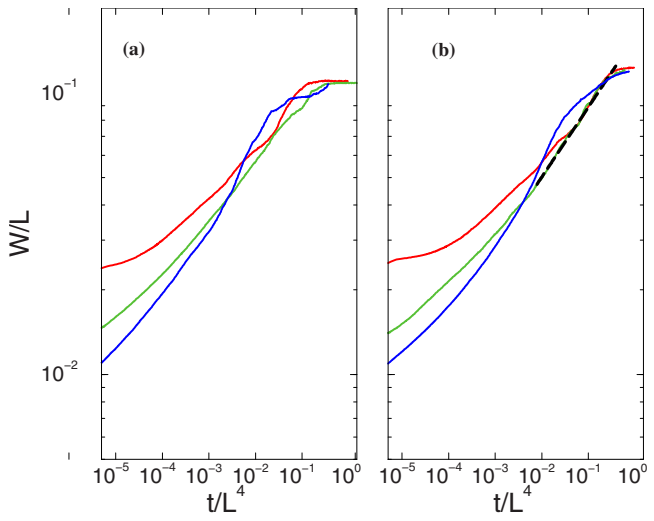

FIG. 3. (Color online) Data collapse of the anisotropic LHOD model assuming MH class exponents for $p_{+x}=1$ (diffusion to the right) with small EW noise (a) $p=q=0.01$ and (b) $p=q=0.005$ for sizes $L=32,64,128$ (top to bottom at the left side). For the growth exponent fitting (dashed line) results in $\beta=0.26(1)$.

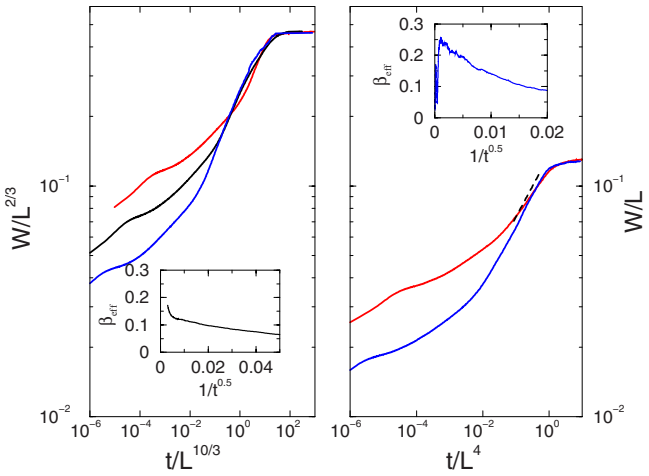

FIG. 4. (Color online) Data collapse of the isotropic LHOD model assuming MBE (left, $l_m=4$) and MH (right, $l_m=3$) class exponents in the presence of small EW noise $p=q=0.005$ in sizes $L=32,64,128$ (top to bottom at the left side). For the growth exponent power-law fitting (dashed line) results in $\beta=0.26(1)$. Inserts show the effective β exponents for $L=64$.

corresponding to $\alpha=1$, and the horizontal scaling improves as we decrease the noise [see Fig. 3(b)]. In opposite, by increasing the amplitude of the EW noise, we can find better collapse with smaller dynamical exponent, describing the crossover to the EW behavior, which has $z=2$. The time dependence shows deviations from the pure scaling law, especially for early times, still before the saturation the growth of $W(t)$ can be fitted with the exponent $\beta=0.26(1)$ [79]. This suggests that in the $p=q \to 0$ limit, the true MH scaling emerges. Simulating larger sizes is very hard because due to the large dynamical exponent z, the saturation is shifted to very late times (for $L=128$, this happens for $t>2\times10^8$ MCS only).

In case of isotropic diffusion, the scaling is MBE class type in general [see Fig. 4(a) for $l_m=4$], characterized by the exponents $\alpha=2/3$, $\beta=0.2$, and $z=10/3$ in two dimensions. Therefore, the algorithm with the LHOD update (18) breaks the detailed balance condition (17) and introduces a nonlinearity. However, this nonlinearity is small and by decreasing l_m, it becomes even smaller [see Fig. 4(b)]. One can find a rather good collapse with the MH exponents in case of $l_m=3$. We estimated the growth exponent by calculating the local slopes

$$\beta_{eff}(t) = \frac{\ln W(t, L \to \infty) - \ln W(t', L \to \infty)}{\ln(t) - \ln(t')}. \qquad (19)$$

As one can read-off from the inserts of Fig. 4, for $l_m=4$, this effective exponent extrapolates to the MBE value [$\beta=0.20(2)$], while for $l_m=3$ to $\beta=0.26(1)$, agreeing with the MH exponent in the $t \to \infty$ limit. This means that the LHOD rule introduces more possibilities for breaking the detailed balance condition (17) when more degrees of freedom (more directions or larger jumps sizes) are allowed. This provides an explanation for the difference between the scaling behavior of the isotropic and anisotropic diffusions. To avoid such

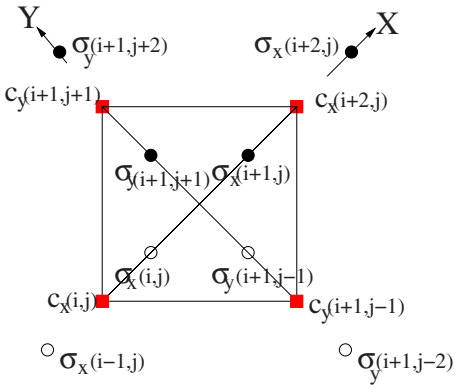

FIG. 5. (Color online) Local slope $\sigma_\chi(i,j)$ (circles) and curvature $c_\chi(i,j)$ (squares) variables at an update site. Filled circles correspond to upward, empty ones to downward slopes of the surface. This plaquette configuration models a valley bottom site, with the total curvature $H=4$.

nonlinearity completely, we introduced a more complex update rule based on the local curvature conditions keeping the spatial symmetries.

B. Larger curvature octahedron diffusion model

In this section, we describe a transition probability in addition to the octahedron surface hopping model, which satisfies the detailed balance condition (17), thus enables one to realize linear, equilibrium MH diffusion steps. The local curvature of the surface is calculated at the four edges of squares of the projected octahedra. As Fig. 5 shows, one can describe the curvatures $c_\chi(i,j)$ $[\chi \in (x,y)]$ by the products (or differences) of the local slopes

$$c_\chi(i,j) = \sigma_\chi(i,j)\sigma_\chi(i+1,j). \tag{20}$$

At each update, we calculate the sum of the change of local curvatures at the origin (i,j) and the target (i',j') sites

$$\Delta H = \Delta \sum_{\chi=x,y} \sum_{\langle i,j \rangle} c_\chi(i,j) + \Delta \sum_{\chi=x,y} \sum_{\langle i',j' \rangle} c_\chi(i',j'), \tag{21}$$

where $\langle\ \rangle$ denotes the plaquette neighborhood sites as shown on Fig. 5. This gives maximal value $H=4$ for a local tops and bottoms and the minimal value $H=-4$ for a locally flat (zigzag) configuration. Using this value, we accept the update with an Arrhenius type of probability

$$w_{i\to i'} = 1/2[1 - a \tanh(-\Delta H^2)], \tag{22}$$

where a is a constant. This form is very similar to what was used in case of the one-dimensional $n=2$ model [42] and enhances (suppresses) roughening moves if $a>0 (a<0)$, respectively. In [42], symmetry arguments were applied for the lowest-order series expansion of $w_{i\to i'}$ of the model to prove a connection with the MH equation. Now, similar derivation can be done by extending the model for dimer variables in two dimensions. In the forthcoming, we shall call this the larger curvature octahedron diffusion (LCOD) model.

We have simulated the LCOD with the parameters $a=0.1$ and $l_m=3$, corresponding to inverse or roughening surface diffusion and $p=q=0.05$. The scaling behavior has been found to agree very well with that of MH universality class values even in case of isotropic diffusion (see Fig. 6). The effective $\beta_{eff}(t)$ converges to $\beta=0.25(1)$ before the saturation. The wavelength grows logarithmically in time (see insert of Fig. 6) and after a steady-state value is reached, it scales logarithmically with the system size too.

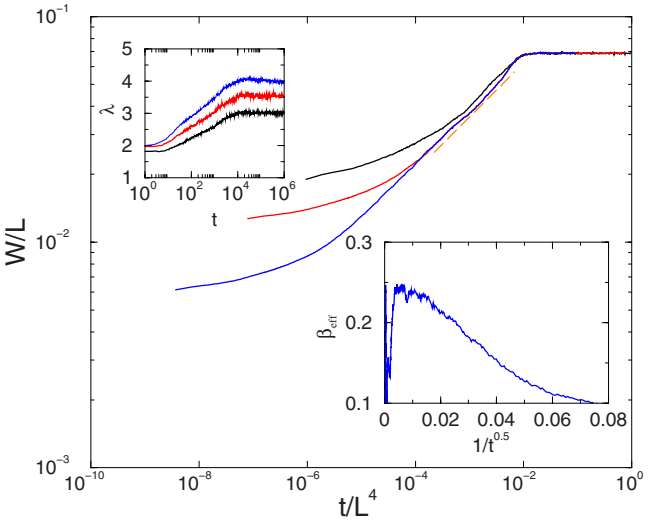

FIG. 6. (Color online) Scaling behavior of the isotropic LCOD model for $L=32,64,128$ (top to bottom at the left side). The data collapse has been achieved with the MH class exponents. For the growth exponent fitting (dashed line) results in $\beta=0.25(1)$. Insert on the right shows the same by local slopes. Insert on the left shows the evolution of λ.

For anisotropic diffusion ($p_{\pm x}=1$, $p_{\pm y}=0$), we have obtained similarly good MH class surface scaling, with logarithmic time and size dependences of λ again. For $a=0$, without any EW noise, one can find logarithmic growth in the LCOD model in time

$$W(t, L\to\infty) \propto \ln(t) \tag{23}$$

and logarithmic surface roughness dependence of

$$W(t\to\infty, L) \propto \ln(L). \tag{24}$$

Data collapse fitting for the dynamical exponent on the other hand results in space-time anisotropy with $z=4$. This means that for the $a=0$ noiseless case, we could realize the universality class behavior of MH with conserved (purely diffusive) noise, characterized by the exponents $\alpha=\beta=0$, $z=4$ (see [16]).

III. PATTERN GENERATION BY COMPETING INVERSE MH AND KPZ PROCESSES

As we have shown in the previous section, in the zero noise limit, our RSOS surface diffusion processes generate growth with MBE or MH scaling behavior. In this section, we investigate them in the presence of competing KPZ updates. In our simulations, we initiate hopping with probabilities p_{+x}, p_{-x}, p_{+y}, and p_{-y} alternately with the deposition (with probability p) and removal (with probability q) pro-

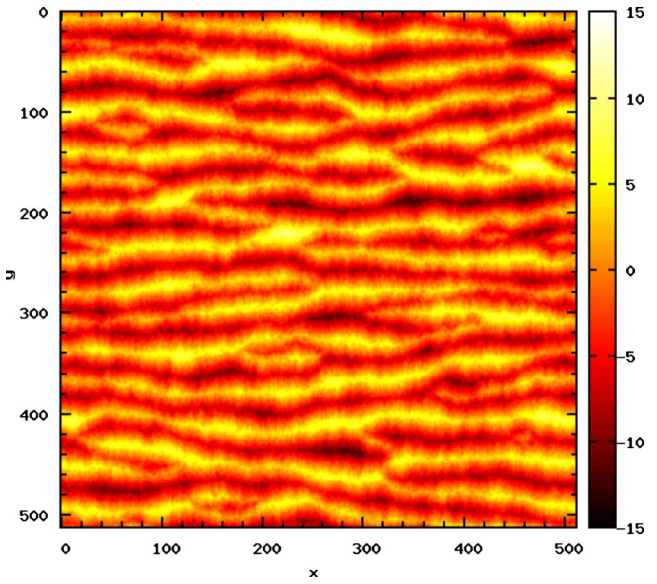

FIG. 7. (Color online) Snapshot of surface heights of the ripple patterns generated by the parameters $p_{\pm x}=1$, $p_{\pm y}=0$ (anisotropic, inverse MH) and $p=q=1$ adsorption or desorption at $t=10^4$ MCS in the LHOD model of linear size $L=512$.

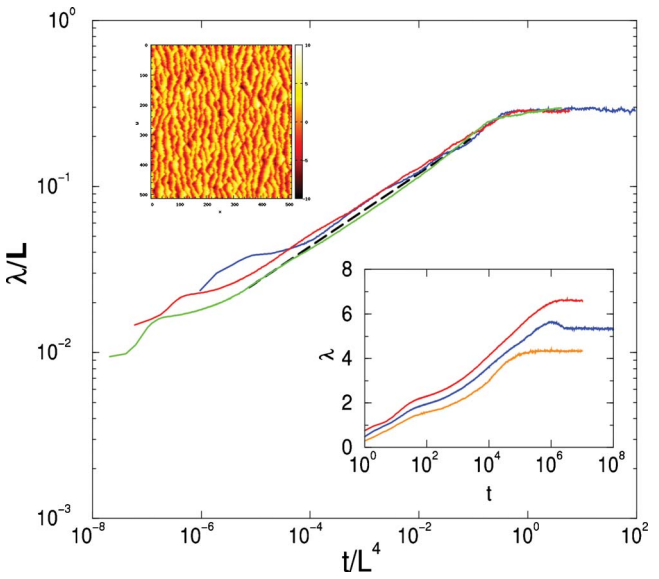

FIG. 8. (Color online) Wavelength growth in the LHOD model for anisotropic diffusion with steady dc current $p_{+y}=1$, $p=q=0.005$ for sizes $L=32,64,128$ (top to bottom at the beginning). (Dashed line) Power-law fit with the exponent $\beta=0.24(1)$. Left insert shows the corresponding pattern. Right insert corresponds the isotropic diffusion case $p_{\pm x}=p_{\pm y}=1$, where $\lambda(t)$ grows logarithmically.

cesses. We follow the surface roughness and pattern formation with the corresponding wavelength growth.

A. Spatially anisotropic surface diffusion

From the point of pattern formation, the LHOD and LCOD models behave differently. We always start the simulations from a flat surface and watch if stable patterns can arise. In case of an anisotropic inverse LHOD model of diffusion probability $p_{\pm x}=1$, $p_{\pm y}=0$, a competing EW process always generates ripple patterns as shown on Fig. 7, which is stable for all $p=q\leq 1$. This formation is metastable against KPZ (height anisotropy), but for very large times (in the steady state), the ripples become uneven, blurred, and cut into smaller pieces. The wavelength, defined as Eq. (10) grows only a little (in a power-law manner) and saturates quickly.

However, if we create such anisotropy in which a steady, direct current (dc) flows, for example, when only $p_{+x}=1$ and all the others are zero, we can find a different behavior. In this case, for weak EW or KPZ, the ripples are not completely straight and exhibit a coarsening as

$$\lambda \propto t^{0.24(1)}. \tag{25}$$

The ripples are straighter in the KPZ case than for up-down isotropic deposition or removal. Furthermore, a good data collapse can be obtained with the MH class exponents for sizes $L=32,64,128$ as shown on Fig. 8. However, this scaling can be destroyed by increasing the strength of the nonconserved reaction and the power-law crosses over to logarithmic growth of λ. In case of strong KPZ deposition ($p=1$, $q=0$), the asymptotic scaling of the LHOD becomes completely KPZ type, the wavelength saturates very quickly (see Fig. 9), and the ripple structure smears. In principle, we should expect anisotropic KPZ behavior here, but it is well known that in two dimensions, such spatial anisotropy is irrelevant, hence the isotropic KPZ class behavior [65] is not surprising. Note that our anisotropic KS model is different from what is called and considered to be the "anisotropic KS" in the literature [66] because in our case, the surface diffusion (corresponding to the ∇^4 term) is anisotropic. Such models are very hard for analytic treatment and spatial anisotropy is introduced in the ∇^2 terms usually.

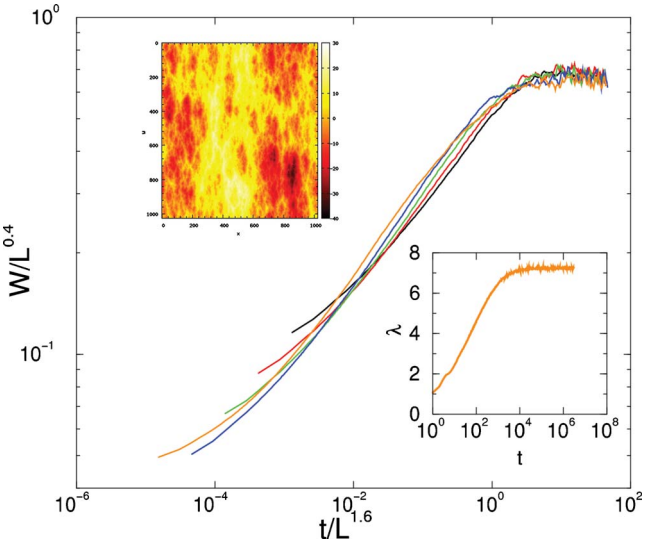

FIG. 9. (Color online) Data collapse for deposition ($p=1$, $q=0$) and anisotropic, inverse diffusion $p_{\pm y}=1$ in the LHOD model with KPZ class exponents for $L=64,128,256,512,1024$ (top to bottom curves at the right side). (Right insert) $\lambda(r)$ for $L=1024$. (Left insert) Blurred ripple structure.

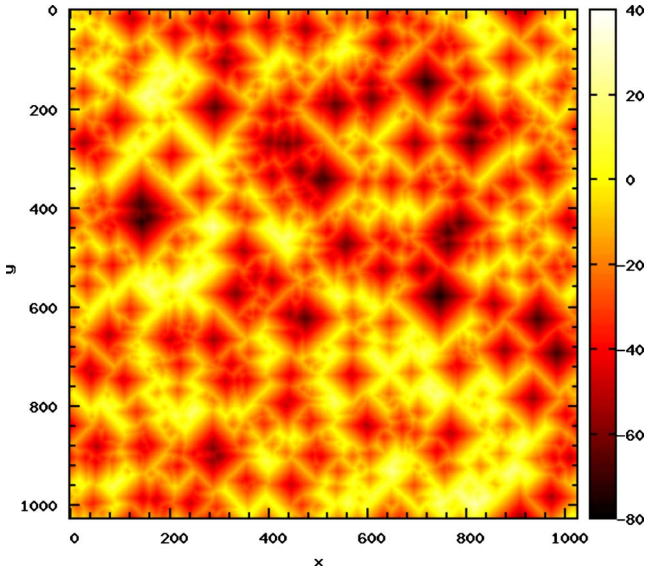

FIG. 10. (Color online) Snapshot of surface heights of the dot patterns generated by the LHOD model with parameters $p_{\pm x}=p_{\pm y}=1$ (isotropic, inverse MH) and $p=q=0.1$ at $t=10^4$ MCS.

The anisotropic LCOD is less effective for ripple formation than the LHOD. In this case, the patterns are smoother and the λ scales logarithmically in time and by the size. The only exception is when we allow a steady dc current again. In this case, similar power laws as shown on Fig. 9 emerge for weak EW or KPZ.

When dc current is not allowed ($p_{\pm x}=1$, $p_{\pm y}=0$), only spatial anisotropy in the LCOD and we add a KPZ ($p=1$, $q=0$) update, we can see the emergence of KPZ scaling. In this case, the wavelength depends logarithmically both on time and the size L. It is important to realize that for short, one decade length, time windows the wavelength growth can also be well fitted with a power law

$$\lambda(t,L\to\infty)\propto t^{0.17(1)}, \tag{26}$$

which resembles to experimental results, but since the steady-state values exhibit a clear logarithmic dependence on the sizes

$$\lambda(t\to\infty,L)\propto \ln(L), \tag{27}$$

we do not think that this "power-law" fit would correspond to a real asymptotic behavior in the thermodynamic limit.

B. Spatially isotropic surface diffusion

When the isotropic, inverse surface diffusion competes with the (smoothing) EW process, one can observe dot formation both in the LHOD and LCOD models. Figure 10 shows a snapshot of the growing dots for LHOD in the presence of weak EW process. Here, one can see rectangular-shaped patterns corresponding to the lattice symmetry. In case of LCOD, the contrast of the patterns is smoother, roughly circular. However, this pattern coarsening is much slower than in case of ripples.

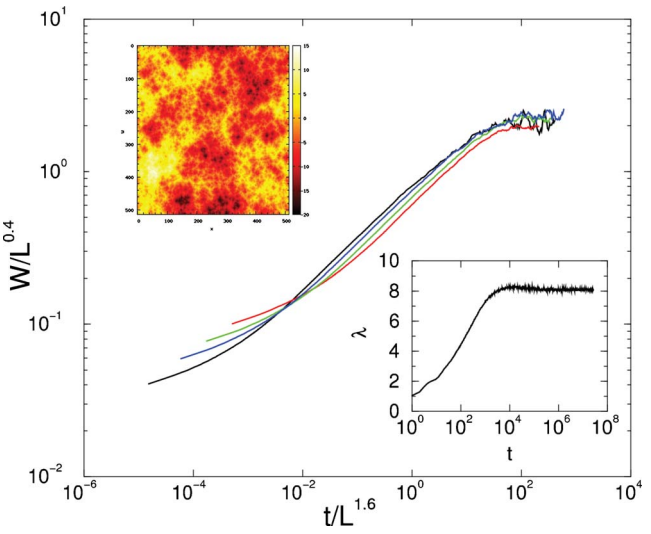

FIG. 11. (Color online) Data collapse of the $L=128,\ldots,1024$ LHOD model ($p_{\pm x}=p_{\pm y}=1$) with a competing deposition ($p=1$) process. One can see a very slow crossover toward KPZ scaling. Right insert shows the growth of λ for $L=512$. Left insert is a snapshot of the steady state, corresponding to the smeared KPZ height distribution.

We shall discuss the LHOD results first which, according to our previous numerical analysis, corresponds to the nonlinear equation (KPZ+MBE)

$$\partial_t h=\sigma\nabla^2 h+\lambda_2(\nabla h)^2+\nu_4\nabla^4 h+\lambda_{22}\nabla^2[\nabla(h)^2]+\eta. \tag{28}$$

In case of EW type of deposition or removal, the nonlinear term vanishes ($\lambda_2=0$) and in fact we model the CKPZ behavior. The characteristic size (λ) of the dots grows logarithmically (see insert of Fig. 8) in time and $\lambda_{\max}\propto\ln(L)$. The pattern formation is more pronounced in the LHOD case than in the LCOD model. We associate it to the up or down anisotropy present in the LHOD.

The same kind of patterns can be also observed in case of strong KPZ anisotropy $p=1$, $q=0$ for short times, but later the dots are smeared. For the LHOD+KPZ case, a very slow crossover to KPZ scaling (see Fig. 11) occurs. Although the data collapse with KPZ exponents is rather poor for smaller sizes (it would be better with larger z and α exponents corresponding to the MBE class), for $L\geq 512$, it agrees with KPZ. The wavelength saturates very quickly (see insert of Fig. 11) in agreement with KPZ, where no coarsening is expected.

Having confirmed that the LCOD model exhibits MH scaling, now we can investigate the scaling behavior of the (inverse) KS Eq. (16), described by the combination of inverse MH and normal KPZ processes. We have run extensive simulations up to $t=3\times10^6$ MCS (for $L=128,256,512,1024$) to obtain firm numerical evidence. As Fig. 12 shows, the finite-size scaling collapse with KPZ exponents is satisfied and the effective β extrapolates to 1/4. This value agrees well with our high-precision KPZ simulation result [12]. The wavelength grows logarithmically in

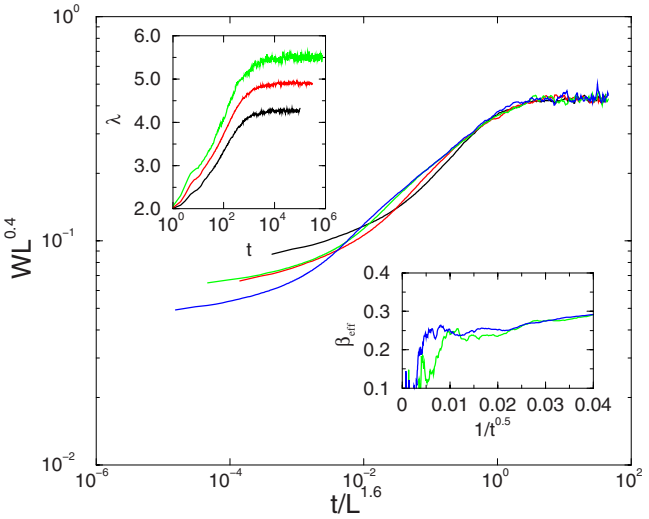

FIG. 12. (Color online) Data collapse of the $L=128,\ldots,1024$ (top to bottom at the right) LCOD model ($p_{\pm x}=p_{\pm y}=1$) with competing deposition ($p=1$). One can see clear KPZ scaling. Left insert shows the logarithmic growth of λ for $L=128,256,512$ (bottom to top). (Right insert) β_{eff} as the function of time.

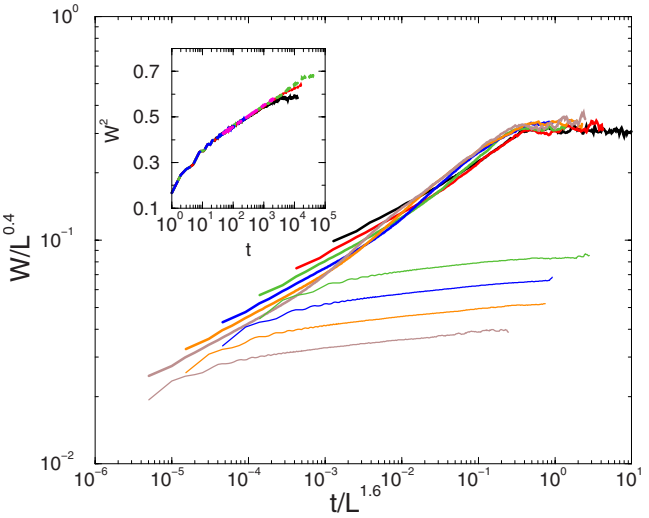

FIG. 13. (Color online) Data collapse of KPZ deposition ($p=1$) and weak, isotropic normal LHOD (higher curves) for $L=64,128,\ldots,2048$ (top to bottom). In case of strong diffusion (lower curves), the KPZ scaling disappears and as the insert shows, logarithmic growth can be observed.

time (26) (see insert of Fig. 12) and saturates well before the steady state. In the steady state, it grows slowly with the system size as Eq. (27). In a 1-decade-long time window, one can fit the data with $\lambda(t,L\to\infty)\propto t^{0.12(2)}$, but due to the clear logarithmic behavior in the steady state (27), one should not take such power-law fitting very seriously.

For the sake of completeness, we have performed similar analysis for the anisotropic LCOD model ($p_{\pm x}=1$, $p_{\pm y}=0$) with KPZ too for sizes $L\leq 1024$. We have obtained agreement with the KPZ scaling for the width W and logarithmic growth for λ as in case of isotropy.

IV. KPZ IN THE PRESENCE OF NORMAL SURFACE DIFFUSION

In this part, we show the scaling behavior study of the KPZ process in the presence of normal (smoothing) LHOD, introduced in the previous section. First let us consider the weak isotropic diffusion case $p_{\pm x}=p_{\pm y}=0.1$. As Fig. 13 shows, the $W(t)$ curves for sizes $L=64,128,\ldots,2048$ exhibit a good collapse when we rescale them with the 2+1-dimensional KPZ exponents (4). This means that the KPZ scaling is stable against the introduction of a smoothing, MBE type of surface diffusion.

On the other hand, when we add strong LHOD diffusion, $p_{\pm x}=p_{\pm y}=0.9$, to the KPZ process ($p=1$), the surface growth slows down and we do not find the KPZ scaling anymore (see the lower part of Fig. 13). Instead, logarithmic surface growth emerges, as shown in the insert of Fig. 13. A fitting with the form $W^2(t)=A+B\ln(t)$ for the asymptotic growth regime gives $A=0.40(1)$ and $B=0.26(1)$. The amplitude of this growth is different from the exactly known universal value of the EW class in two dimensions: $A_{\mathrm{EW}}=0.151\,981$ [67].

The wavelength saturates very quickly to the maximal value, which for weak diffusion scales logarithmically with the system size (27), while in case of the strong diffusion, the characteristic length remains on the order of lattice unit: $\lambda_{\max}\simeq 1$, with a very weak size dependence, corresponding to uncorrelated surface heights (see Fig. 14). It is well known that in the strong diffusion limit, the relevant fluctuations below d_c can be washed away, hence the logarithmic surface growth we observe should correspond to the mean-field behavior of the strong-coupled KPZ. This provides us a unique way to study the crossover behavior between the KPZ and KPZ mean-field behavior.

V. PROBABILITY DISTRIBUTION RESULTS

Here we present the probability distributions $P(W^2)$ obtained in the steady state of our model. Such distributions are universal, hence they complement the previous scaling re-

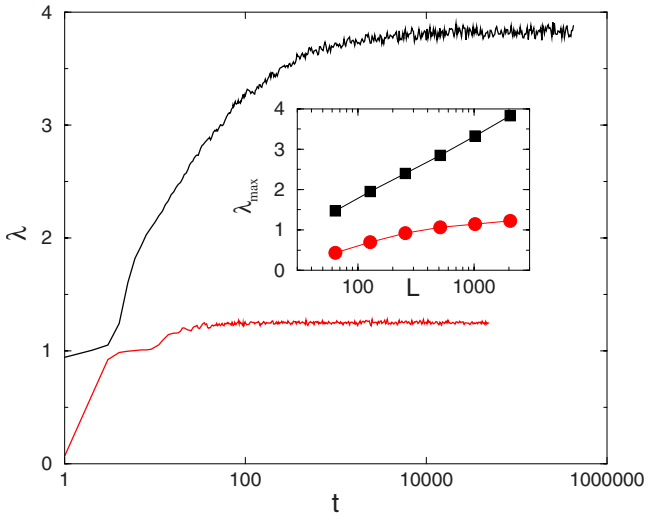

FIG. 14. (Color online) Wavelength saturates quickly for KPZ+weak LHOD (higher curve) and KPZ+strong LHOD (lower curve) diffusion ($L=2048$). Insert shows $\lambda_{\max}$ vs L.

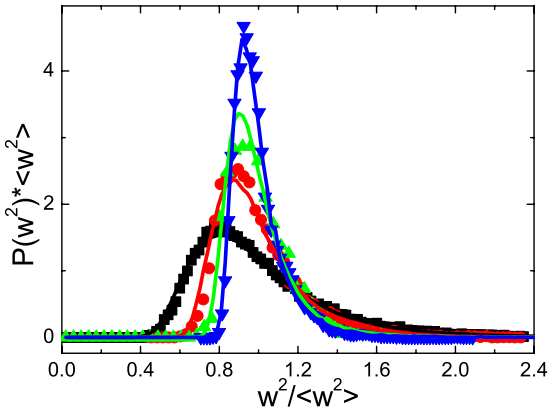

FIG. 15. (Color online) Comparison of the $P(W^2)$ of the higher dimensional octahedron model results (symbols) to those of [69] (lines) in $d=2,3,4,5$ spatial dimensions (bottom to top).

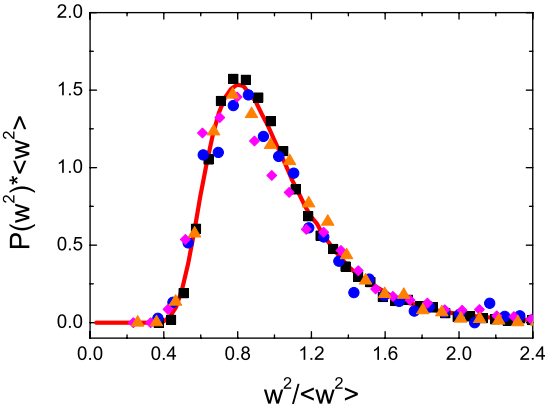

FIG. 16. (Color online) Comparison of $P(W^2)$ of the KPZ +LHOD (black boxes), KPZ+inverse LHOD (blue dots), KPZ +inverse, anisotropic LHOD (pink rhombuses), and KPZ+inverse LCOD (orange triangles) to that of the KPZ from Ref. [69] (solid line).

sults. The exact functional form for KPZ is known in one dimension only, but in two dimensions, very precise numerical data exist, obtained via other surface models [68]. The distributions of those KPZ models have been determined in higher dimensions [69], suggesting the lack of finite upper critical dimension.

First, we compare our $P(W^2)$ results for KPZ to those of [69] in $d=2,3,4,5$ dimensions. The W^2 distribution data were taken from the saturation regimes and analyzed in systems of sizes $L=1024$ (two dimensions, 2d), $L=512$ (three dimensions, 3d), $L=64$ (four dimensions, 4d), and $L=32$ (five dimensions, 5d). The presented data are coming from our higher-dimensional KPZ simulations using the extended octahedron model described in [12]. When we rescaled our data with $\langle W^2 \rangle$ as Fig. 15 shows, we found very good agreement in $d=2,3,4,5$ dimensions with the earlier KPZ distribution curves. Again, we cannot see a signal for an upper critical dimension at $d_c=4$, conjectured by theoretical approaches (see, for example, [70]).

Furthermore, we tested our surface-scaling results for KPZ within the presence of diffusion. In case of competing KPZ and LHOD or LCOD processes (i.e., for $p=1$, $q=0$, $p_{\pm x}=p_{\pm y}=1$), we determined the $P(W^2)$ distributions well in the saturation regime of systems of size $L=1024$. The steady state could be reached for $t>\sim 10^5$ MCS in case of KPZ +LHOD and for $t>5\times 10^7$ MCS in case of the KPZ +LCOD model. We generated 100 independent samples and cut out the steady-state data of $W^2(t)$. We calculated the scaled steady-state probability distributions as shown on Fig. 16 for different combinations. The comparison to the histogram of the 2+1-dimensional KPZ from [69] shows a good agreement in general, providing further numerical evidence that the KS model asymptotically exhibits the KPZ universality class scaling. Our results complement the one-dimensional simulations results of [61], in which the equivalence of KS and KPZ scalings was confirmed numerically.

VI. CONCLUSIONS AND OUTLOOK

We have returned to some unresolved questions of basic surface growth phenomena using extensive computer simulations of atomistic models. Contrary to earlier studies, we could perform numerical analysis of models with surface diffusion in 2+1 dimensions due to the effective mapping of RSOS models onto binary lattice gases.

We have shown that in the zero external noise limit, RSOS models with short-range interactions can be constructed, which exhibit molecular-beam epitaxy or Mullins-Herring type of surface growth. For inverse (roughening) diffusion, which increases the local curvature, unstable growth resulting in pyramidlike structures emerges. The size of these structures is limited only by L, which is not directly comparable to real materials. We created these MBE or MH type of atomistic models in order to study them in a competition with nonconserved KPZ processes. The simulations provided numerical evidence that strong, smoothing surface diffusion can slow down the KPZ to a logarithmic growth, thus we are able to reach the mean-field behavior of the strongly coupled KPZ fixed point in two dimensions, which is expected to show up in high dimensions only.

The mapping of the surface models onto lattice gases implies that the (anisotropic) oriented diffusion of dimers (KPZ) is stable against the introduction of an attracting force among them, but a strong repulsion can destroy the fluctuations, resulting in a mean-field behavior. We provided strong numerical evidence using surface scaling and probability distribution studies that the KS model exhibits KPZ scaling in 2+1 dimensions as conjectured by field theory. We summarized the models we considered in case of spatially isotropic surface diffusion and nonconserved noise in Table I.

Further studies of LCOD, with different boundary conditions, can set the target of the research of the surface inclination by mapping the surface tilt onto the total particle concentration of the lattice gas. In particular, the angle dependence of the phase transitions among different growth phases can be understood by considering the underlying driven gas. Using our method, one can transform results of disorder or of anomalous diffusion between the surface and lattice-gas models.

We presented a characteristic length scale λ to follow the dynamics of patterns, which occur, if normal (smoothing)

TABLE I. Overview of the surface models with spatial isotropy and nonconserved noise. Columns 2–5 show the sign of couplings of the differential equations considered.

Model acronym	σ	λ_2	λ_{22}	ν_4	Properties
EW	+	0	0	0	Smooth surface (logarithmic) growth
KPZ	+	+/−	0	0	Rough surface (power-law) growth
MH	0	0	0	+	Smoothing diffusion, $z=4$
iMH	0	0	0	−	Inverse/roughening diffusion, unstable, $z=4$
MBE	0	0	+/−	+	Normal/smoothing diffusion, $z=10/3$
iMBE	0	0	+/−	−	Inverse/roughening diffusion, $z=10/3$, pyramids
KS	+	+/−	0	−	KPZ scaling, dot pattern (logarithmic) growth
iKS	+	+/−	0	+	KPZ scaling, mean-field for strong diffusion

KPZ competes with inverse (roughening) diffusion. We investigated this race for MH and MBE process, with and without spatial anisotropies. In case of uniaxial surface diffusion ripple, while for x/y lattice isotropy, dotlike pattern formation could be achieved. The wavelength growth is slow and saturates much before the steady state. Usually, we found logarithmic time and system size dependence of λ, except when steady dc current flows through the system. In this case, the interfaces are more rough, the ripples are bended, and power-law scaling is observable. In this case, the scaling of λ agrees with the scaling of the width, i.e., characterized by the MH class exponents. This finding agrees with 3d kinetic Monte Carlo simulations of epitaxial growth and erosion on (110) crystal surfaces [71] and with analytic arguments [72]. Furthermore, in case of ion beams with grazing incidence, the dislocation dynamics results in such athermal, kinetic coarsening of the patterns [73].

The wavelength behavior can be understood with the help of considering the underlying lattice-gas model, since the ripple or dot structures correspond to a phase separation. The coalescing surface pattern dynamics can be mapped onto the generalization of the reaction-diffusion process [16] of extended objects. It was shown that in ASEP type of models, where strong phase separation is present, the domain growth follows slow, logarithmic behavior [74,75] in case of smooth surfaces. On the other hand, for rough surfaces, power-law coarsening of λ has been derived using simple scaling arguments [76]. Finally, we mention that our models enable effective, bit-coded, stochastic cellular automaton type of simulation of surfaces, hence they could be run extremely fast on advanced graphic cards.

ACKNOWLEDGMENTS

We thank Zoltán Rácz for the useful comments and providing us universal probability distribution functions $P(W)$ of other KPZ models. Supports from the Hungarian research fund OTKA (Grant No. T046129) and the bilateral German-Hungarian exchange program DAAD-MÖB (Grants No. D/07/00302 and No. 37-3/2008) are acknowledged. The authors thank for the access to the HUNGRID, Cluster-grid, and the NIIF supercomputer in Budapest.

[1] S. Facsko, T. Dekorsy, C. Koerdt, C. Trappe, H. Kurz, A. Vogt, and H. L. Hartnagel, Science **285**, 1551 (1999).
[2] M. Makeev, R. Cuerno, and A.-L. Barabási, Nucl. Instrum. Methods Phys. Res. B **197**, 185 (2002).
[3] T. Halpin-Healy and Y.-C. Zhang, Phys. Rep. **254**, 215 (1995).
[4] A. L. Barabási and H. E. Stanley, *Fractal Concepts in Surface Growth* (Cambridge University Press, Cambridge, England, 1995).
[5] M. Kardar, G. Parisi, and Y. C. Zhang, Phys. Rev. Lett. **56**, 889 (1986).
[6] D. Forster, D. R. Nelson, and M. J. Stephen, Phys. Rev. A **16**, 732 (1977).
[7] H. van Beijeren, R. Kutner, and H. Spohn, Phys. Rev. Lett. **54**, 2026 (1985).
[8] H. K. Janssen and B. Schmittmann, Z. Phys. B **63**, 517 (1986).
[9] M. Kardar, Nucl. Phys. B **290**, 582 (1987).
[10] T. Hwa, Phys. Rev. Lett. **69**, 1552 (1992).
[11] G. Ódor, B. Liedke, and K.-H. Heinig, Phys. Rev. E **79**, 021125 (2009).
[12] G. Ódor, B. Liedke, and K.-H. Heinig, Phys. Rev. E **81**, 031112 (2010).
[13] S. F. Edwards and D. R. Wilkinson, Proc. R. Soc. London, Ser. A **381**, 17 (1982).
[14] H. Hinrichsen and G. Ódor, Phys. Rev. Lett. **82**, 1205 (1999).
[15] G. Ódor, Rev. Mod. Phys. **76**, 663 (2004).
[16] G. Ódor, *Universality in Nonequilibrium Lattice Systems* (World Scientific, Singapore, 2008).
[17] A. J. Bray, Adv. Phys. **43**, 357 (1994).
[18] M. Castro, A. Hernandez-Machado, and R. Cuerno, Phys. Rev. E **79**, 021601 (2009).
[19] A. Keller, R. Cuerno, S. Facsko, and W. Moller, Phys. Rev. B **79**, 115437 (2009).
[20] J. Munoz-Garcia, R. Gago, L. Vazquez, J. A. Sanchez-Garcia, and R. Cuerno, Phys. Rev. Lett. **104**, 026101 (2010).
[21] M. Plischke, Z. Rácz, and D. Liu, Phys. Rev. B **35**, 3485 (1987).

[22] P. Meakin, P. Ramanlal, L. M. Sander, and R. C. Ball, Phys. Rev. A **34**, 5091 (1986).
[23] T. Ligget, *Interacting Particle Systems* (Springer-Verlag, Berlin, 1985).
[24] B. Schmittman and R. K. P. Zia, in *Phase Transitions and Critical Phenomena*, edited by C. Domb and J. L. Lebowitz (Academic Press, London, 1996), Vol. 17.
[25] J. Marro and R. Dickman, *Nonequilibrium Phase Transitions in Lattice Models* (Cambridge University Press, Cambridge, England, 1999).
[26] M. Lässig, Phys. Rev. Lett. **80**, 2366 (1998).
[27] F. Family and T. Vicsek, J. Phys. A **18**, L75 (1985).
[28] J. Krug, Adv. Phys. **46**, 139 (1997).
[29] J. M. López and M. A. Rodríguez, Phys. Rev. E **54**, R2189 (1996).
[30] M. Matsumoto *et al.* J. Univers. Comput. Sci. **12**, 672 (2006).
[31] C. Herring, J. Appl. Phys. **21**, 301 (1950).
[32] W. W. Mullins, J. Appl. Phys. **28**, 333 (1957).
[33] M. Constantin, C. Dasgupta, P. Punyindu Chatraphorn, S. N. Majumdar, and S. Das Sarma, Phys. Rev. E **69**, 061608 (2004).
[34] S. Das Sarma, P. P. Chatraphorn, and Z. Toroczkai, Phys. Rev. E **65**, 036144 (2002).
[35] A. Bru, J. M. Pastor, I. Fernaud, I. Bru, S. Melle, and C. Berenguer, Phys. Rev. Lett. **81**, 4008 (1998).
[36] S. Morel, J. Schmittbuhl, J. M. Lopez, and G. Valentin, Phys. Rev. E **58**, 6999 (1998).
[37] S. Das Sarma, S. V. Ghaisas, and J. M. Kim, Phys. Rev. E **49**, 122 (1994).
[38] M. Castro, R. Cuerno, A. Sanchez, and F. Dominguez-Adame, Phys. Rev. E **57**, R2491 (1998).
[39] J. Krug, Phys. Rev. Lett. **67**, 1882 (1991).
[40] J. M. Kim and S. Das Sarma, Phys. Rev. Lett. **72**, 2903 (1994).
[41] J. Krug, Phys. Rev. Lett. **72**, 2907 (1994).
[42] M. Siegert and M. Plischke, Phys. Rev. E **50**, 917 (1994).
[43] F. Family, J. Phys. A **19**, L441 (1986).
[44] D. Wolf and J. Villain, Europhys. Lett. **13**, 389 (1990).
[45] S. Das Sarma and P. Tamborenea, Phys. Rev. Lett. **66**, 325 (1991).
[46] Y. Kim, D. K. Park, and J. M. Kim, J. Phys. A **27**, L533 (1994).
[47] C. Dasgupta, S. Das Sarma, and J. M. Kim, Phys. Rev. E **54**, R4552 (1996).
[48] Y. Kuramoto and T. Tsuzuki, Prog. Theor. Phys. **55**, 356 (1976).
[49] G. I. Sivashinsky, Acta Astronaut. **6**, 569 (1979).
[50] R. Cuerno and K. B. Lauritsen, Phys. Rev. E **52**, 4853 (1995).
[51] J. T. Drotar, Y.-P. Zhao, T.-M. Lu, and G.-C. Wang, Phys. Rev. E **59**, 177 (1999).
[52] I. Procaccia, M. H. Jensen, V. S. Lvov, K. Sneppen, and R. Zeitak, Phys. Rev. A **46**, 3220 (1992).
[53] C. Jayaprakash, F. Hayot, and R. Pandit, Phys. Rev. Lett. **71**, 12 (1993).
[54] V. S. L'vov and I. Procaccia, Phys. Rev. Lett. **69**, 3543 (1992).
[55] V. S. L'vov and V. V. Lebedev, Europhys. Lett. **22**, 419 (1993).
[56] V. S. L'vov and I. Procaccia, Phys. Rev. Lett. **72**, 307 (1994).
[57] C. Jayaprakash, F. Hayot, and R. Pandit, Phys. Rev. Lett. **72**, 308 (1994).
[58] Z. Rácz, M. Siegert, D. Liu, and M. Plischke, Phys. Rev. A **43**, 5275 (1991).
[59] J. Krug, M. Plischke, and M. Siegert, Phys. Rev. Lett. **70**, 3271 (1993).
[60] M. Rost and J. Krug, Physica D **88**, 1 (1995).
[61] J. Krug and F. Hontinfinde, J. Phys. A **30**, 7739 (1997).
[62] R. Metzler and J. Klafter, Phys. Rep. **339**, 1 (2000).
[63] M. Nicoli, R. Cuerno, and M. Castro, Phys. Rev. Lett. **102**, 256102 (2009).
[64] C. A. Haselwandter and D. D. Vvedensky, Phys. Rev. Lett. **98**, 046102 (2007).
[65] U. C. Täuber and E. Frey, Europhys. Lett. **59**, 655 (2002).
[66] S. Facsko, T. Bobek, A. Stahl, H. Kurz, and T. Dekorsy, Phys. Rev. B **69**, 153412 (2004).
[67] T. Nattermann and L.-H. Tang, Phys. Rev. A **45**, 7156 (1992).
[68] Z. Rácz and M. Plischke, Phys. Rev. E **50**, 3530 (1994).
[69] E. Marinari, A. Pagnani, G. Parisi, and Z. Rácz, Phys. Rev. E **65**, 026136 (2002).
[70] H. C. Fogedby, Phys. Rev. Lett. **94**, 195702 (2005).
[71] L. Golubovic, A. Levandovsky, and D. Moldovan, Phys. Rev. Lett. **89**, 266104 (2002).
[72] L. Golubovic and A. Levandovsky, Phys. Rev. E **77**, 051606 (2008).
[73] H. Hansen, A. Redinger, S. Messlinger, G. Stoian, J. Krug, and T. Michely, Phys. Rev. Lett. **102**, 146103 (2009).
[74] M. R. Evans, Y. Kafri, H. M. Koduvely, and D. Mukamel, Phys. Rev. E **58**, 2764 (1998).
[75] Y. Kafri, D. Biron, M. Evans, and D. Mukamel, Eur. Phys. J. B **16**, 669 (2000).
[76] M. R. Evans, Y. Kafri, E. Levine, and D. Mukamel, Phys. Rev. E **62**, 7619 (2000).
[77] Cubic nonlinearity is also possible by the same symmetries, however, not much realization or occurrence has been found.
[78] The opposite, positive ν_4 case corresponds to normal, smoothing surface diffusion.
[79] Note however that for $\alpha \geq 1$, anomalous scaling also occurs, which we do not study here.